Axial Flux Permanent Magnet Generators for Direct-Drive Wind Turbines - Review and Optimal Design Studies

Matin Vatani, *Graduate Student Member, IEEE*, Ali Mohammadi, *Member, IEEE*, Donovin D. Lewis, *Graduate Student Member, IEEE*, John F. Eastham, *RAEng, Fellow*, and Dan M. Ionel, *Fellow, IEEE*

***Abstract*—This paper presents a comprehensive analysis of the feasibility, cost, and electromagnetic performance of five distinct types of axial flux permanent magnet (AFPM) generators designed for direct-drive wind turbines. The generator configurations investigated include a single-sided AFPM generator with a surface-mounted PM rotor (AFPMG), a double-sided AFPM generator featuring PMs on the stator and a reluctance rotor (AFPMG-RR), a coreless stator AFPM generator with surface PMs (CAFPMG-SPM), and a coreless stator AFPM generator with a Halbach PM array rotor (CAFPMG-Hal). Each generator's operating principles and configurations are thoroughly explained and compared. Large-scale multi-objective design optimizations were conducted on each type, taking advantage of symmetric computational models and using a differential evolution algorithm based on 3D finite element analysis (FEA) to minimize cost and mass while maximizing efficiency for all designs. A comprehensive discussion of the optimization results highlights the merits of each configuration. The findings indicate and confirm that AFPM generators can potentially achieve superior performance compared to their radial counterparts, as reported in the literature, while also benefiting from more robust and compatible mechanical integration with wind turbines.**

***Index Terms*—Axial flux PM machines, coreless AFPM, Halbach array, 3D FEA, axial flux switching, differential evolution, direct-drive wind turbine.**

I. Introduction

Wind power generation has become a critical component in the global transition to renewable energy, driven by its potential to reduce carbon emissions and dependence on fossil fuels. As a clean and sustainable energy source, wind power is increasingly being integrated into national grids to combat climate change and meet growing energy demands.

According to the International Renewable Energy Agency (IRENA), wind power capacity has seen rapid growth, accounting for a significant share of global renewable electricity generation in recent years [1]. Advances in wind turbine (WT) technology, such as the development of more efficient generators and improved aerodynamics, have enhanced the energy output and economic viability of wind farms, making them a competitive alternative to traditional power sources [2].

The growing global demand for renewable energy, particularly wind power, has prompted manufacturers to focus on increasing the power output of wind turbine generators. In traditional geared generators, high-power turbines are often coupled with gearboxes to convert the low rotational speed of the turbine to the higher speed desirable for synchronous generators [3]. Studies have shown that gearboxes are prone to shorter lifespans than the wind turbine generators, resulting in frequent maintenance and higher operational costs [4].

To address these challenges, direct-drive wind turbine generators, which do not rely on gearboxes, have gained significant attention [5]. These systems offer several advantages over their geared counterparts, including reduced maintenance costs and improved reliability [6]. Removal of the gearing also enhances the overall efficiency of wind energy systems according to [7], which can improve the performance of wind farms and their economic viability.

Direct-drive wind turbines operate without gearbox at relatively low speeds, requiring large generators to achieve the necessary torque. Consequently, maximizing power output while minimizing generator mass is crucial [8]. Permanent magnet synchronous generators (PMSGs), known for their high power density, are well-suited for this application as they can deliver the required power with a more compact design, making them the primary choice for direct-drive wind turbine generator systems [9].

Axial flux PM machines offer a promising approach to further reducing generator mass, as they can achieve higher power output in a more compact configuration compared to prevalent radial flux machines [10], [11]. Beyond their potential to reduce mass, AFPM generators also facilitate more straightforward direct integration with the wind turbine rotor, reducing the complexity and cost of mechanical components [12]. A design exemplifying the benefits of this integration for a large AFPM generator in wind turbines is detailed in [13].

Challenges in AFPM machines may include high normal forces and complex assembly, while their advantages include a unique form factor for the rotor hub and nacelle, as exemplified in [14]. Although AFPM machines generally have

Matin Vatani, Ali Mohammadi, Donovin, D. Lewis, and Dan M. Ionel are with SPARK Lab, Stanley and Karen Pigman College of Engineering, University of Kentucky, Lexington, KY, USA (e-mail: matin.vatani@uky.edu; ali.mohammadi@ieee.org, donovin.lewis@uky.edu; dan.ionel@ieee.org).

John F. Eastham is with the Department of Electronic and Electrical Engineering, University of Bath, Claverton Down, Bath, BA2 7AY, UK (e-mail: jfeastham@aol.com).

larger outer diameters compared to their radial flux counterparts, their compact form factor allows for multiple stacked AFPM generators on the same shaft, substantially increasing overall power output. Additionally, AFPM generators present enhanced manufacturing modularity and segmentation capability compared to radial flux ones, as demonstrated in [15]. This feature is particularly advantageous for direct-drive wind turbine generators, as it significantly impacts transportation, installation, and maintenance.

This paper, which extends previous work in [16], systematically compares five distinct AFPM generator topologies. Namely coreless stator designs with surface-mounted and Halbach array PM rotor types, a single-sided conventional structure with a surface-mounted PM rotor at two pole-to-slot ratios, and a version with a double-sided reluctance rotor and combined PM and AC excitation on the stator. Each generator topology is optimized for identical power and speed ratings using a combined differential evolution algorithm and 3D finite element analysis (FEA). The optimization results form the foundation for a detailed analysis and comparison of these generator types in terms of mass, cost, and efficiency.

This work makes several key contributions. It provides a comprehensive literature review on AFPM generators for direct-drive wind turbines, highlighting their inherent electromagnetic and mechanical advantages while examining advancements in the field. To optimize the proposed generator topologies for the same power rating, a novel and highly flexible optimization algorithm is introduced, aligning with AFPM machine design principles by treating the outer diameter as a dependent variable of the rated power and maintaining constant current loading to facilitate natural cooling. Furthermore, unlike conventional approaches that assume a fixed pole number, this study considers the pole number as an independent variable in the optimization process. By employing complex 3D FEA modeling, the impact of pole number variations on generator performance is thoroughly investigated, leading to a more refined and effective design methodology. These contributions collectively enhance the design and optimization of AFPM generators, improving their applicability for direct-drive wind turbine systems.

The paper is organized as follows: Section II provides a brief literature review of AFPM generators. Section III describes the AFPM generator topologies under investigation and outlines their fundamental operating principle. Section IV explains the problem formulation, specifying the optimization objectives for the coreless AFPM designs, including a focus on minimizing loss and active mass across all topologies. Section V presents the results of the multi-objective optimization, including an analysis of Pareto fronts for cost and pole count, along with experimental validation of the FEA models.

II. Literature Review

Several previous research projects have assessed and analyzed the performance of AFPM generators with various topologies for direct-drive wind turbines. Muljadi *et al.* [12] introduced a three-layer AFPM generator design, each layer representing one phase. This configuration offers a high degree of modularity, facilitating simplified manufacturing, transportation, installation, and maintenance processes. However there can be minor phase unbalance due to the different radial positions of the phases. The study highlights the advantages of axial flux construction over radial flux designs, particularly in enabling the stacking of multiple stages to increase rated power without altering the outer diameter.

In another example by Chalmers *et al.* [17], an axial flux generator featuring a slotless stator and double-sided surface-mounted PM rotors was proposed. This topology minimizes cogging torque, torque ripple, and noise while enhancing the ratios of power to mass and volume attributed to the absence of stator teeth. Additionally, the normal force between the stator and rotor is more balanced when compared to a toothed stator, potentially reducing the mass of mechanical components.

Vestas Wind Systems introduced an innovative AFPM generator concept in 2012, which was designed for large direct-drive wind turbine with outer diameters exceeding 5 meters [15]. The generator features a multi-toothed structure with armature windings and field excitation on the stator. The stator slots are occupied by the armature windings, while PMs are mounted on top of these slots. The rotor consists of ferromagnetic segments embedded within a non-ferromagnetic plate. The stator comprises multiple linear machine segments distributed around the generator's periphery, incorporating rectangular slots and teeth. This design significantly simplifies the manufacturing and maintenance process of large wind turbines. Furthermore, the patent also explored variations in which the PMs are replaced by field windings on the stator.

More recent efforts have aimed to reduce generator mass further, leading to the development of designs featuring coreless stator configurations. Coreless stator designs are structurally similar to conventional AFPM generators, with the notable distinction of having no stator core, which substantially decreases the mass of active materials. Jean-Sola *et al.* demonstrated that the absence of a ferromagnetic stator core reduces the normal force between the stator and rotor, allowing for a substantially lighter mechanical components [18]. Although a normal force persists between the two rotors, it can be effectively managed by incorporating a C-shaped rotor core, as outlined in [19].

Beyond the relatively lower mass, coreless stator AFPM generators exhibit low starting torque, reduced vibration, and potentially high efficiency, making them highly suitable for direct-drive wind turbines [20]. Muller *et al.* developed multi-stage coreless AFPM generators for direct-drive wind turbines across various power ratings, including a 1 MW demonstrator operating at 12 rpm with an outer diameter of 6.4 meters [21], [22]. The generator topology comprises N concentrated three-phase air-cored winding stators sandwiched between $N+1$ surface-mounted PM rotors.

Boulder Wind Power, supported by funding from the US Department of Energy (DOE), developed a single-stage coreless stator AFPM generator with a rated power of 6 MW and an outer diameter of 20 meters [14]. The stator design utilizes

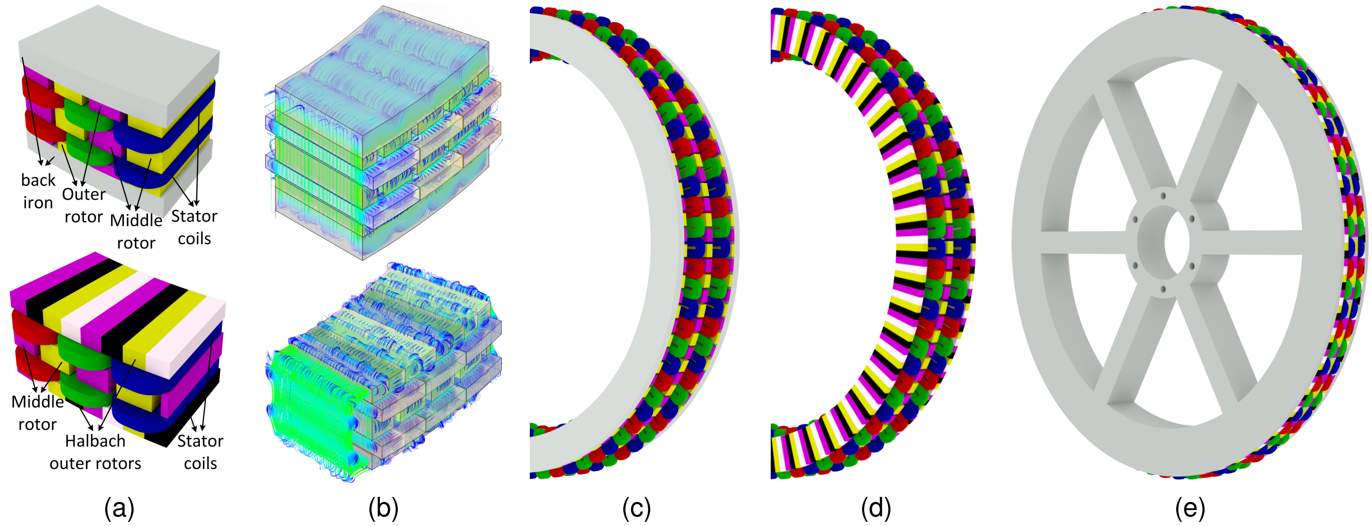

Fig. 1. Coreless stator axial flux permanent magnet generator (CAFPMG) concepts with surface-mounted and Halbach array PM rotors proposed for direct-drive wind turbines. (a) highlights the labeled active components; (b) shows the flux density distribution, with the rotor back iron removed in the Halbach array PM variant; (c) and (d) present slightly exploded views of the two configurations in an example design; and (e) illustrates a simplified mechanical structure for the Halbach array rotor variant, incorporating composite materials.

printed circuit board (PCB) materials based on the concept first introduced in [23]. This PCB-based approach accelerates production, minimizes human error through automation, and significantly reduces costs compared to Litze wire, particularly in mass production scenarios.

While coreless stator AFPM generators reduce the mass of both active and inactive components, they require a larger volume of magnets to compensate for the lower flux density in the airgap compared to their conventional cored counterparts, which can significantly raise costs. Alternatively, if magnet volume is limited to the same values as a cored AFPM generator of the same size, the coreless design produces less power. Consequently, AFPM generators with coreless stators often have larger dimensions than similarly rated cored stator designs, which may even result in a heavier generator.

III. Generator Topologies

The applications of the generators introduced in the following sections are not limited to wind turbine generators; similar variations can also be found in applications such as vehicles, aircraft, and HVAC systems, as discussed in [24]–[26]. Adapting these generators for different applications requires modifications in topology and design objectives to meet the specific requirements of each scenario. For instance, core and conductor eddy current losses in high-speed applications can become significant, necessitating topology modifications and design constraints to mitigate these effects.

A. Coreless Stator AFPM Generators

The coreless stator axial flux permanent magnet generators (CAFPMGs) considered in this paper employ single-layer PCB stators positioned between three rotors—two outer rotors and one middle rotor. For the outer rotor, two designs are considered: one with a conventional surface-mounted PM (SPM) rotor and the other with a Halbach array PM rotor, as shown in Figs. 1(c) and 1(d). In the SPM rotor, magnets with alternating polarity are mounted on a ferromagnetic back iron, which serves as the flux return path. The Halbach array rotor, by contrast, is composed of four magnets per wavelength (two pole pitches), where the magnetization direction of consecutive magnets differs by 90 degrees.

The middle rotor has the same configuration in both CAFPMGs and consists of normally magnetized magnets embedded in a non-ferromagnetic plate. This rotor has the same pole number as the outer rotors and guides magnetic flux from one outer rotor to another. The proposed CAFPMG topologies are novel, combining a multi-disk configuration with PCB stators for direct-drive wind turbines.

Three-dimensional (3D) magnetic flux density distribution for a sample design of the proposed CAFPMGs featuring SPM and Halbach outer rotors are illustrated in Fig. 1b. The Halbach array configuration enhances the magnetic flux density on one side of the array while significantly reducing it on the opposite side. This characteristic eliminates the need for a rotor back iron, potentially reducing the active mass of the rotor and improving overall efficiency.

Each stator is designed with a three-phase concentrated winding configuration featuring a coil span of 240 electrical degrees (equivalent to three coils spanning over four poles). As demonstrated by Eastham *et al.* [27], this winding layout achieves the highest winding factor in CAFPM machines, maximizing torque production. The pole-to-coil ratio of 4/3 in coreless AFPM machines corresponds to an 8/6 pole-to-slot ratio in conventional machines, meaning the pole number can be a multiple of four in the proposed CAFPMGs. The stator coils are designed with rectangular copper Litz wire to mitigate eddy current losses. Both stators are identical and can

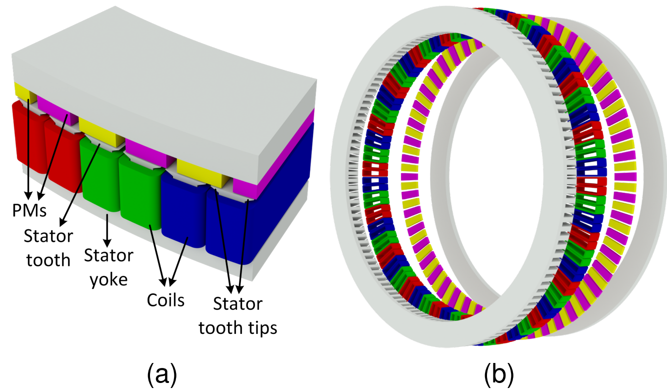

Fig. 2. Conventional single-sided AFPM generator with a 10/12 pole-to-slot ratio (AFPMG-10/12), showing (a) labeled active electromagnetic components and (b) an exploded view of an example design.

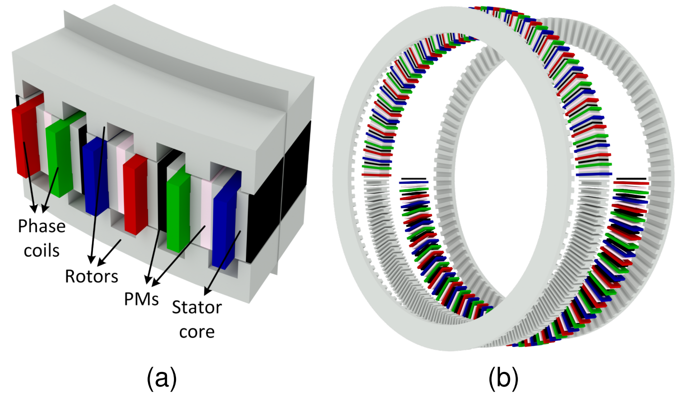

Fig. 4. Axial flux generator concept with combined PM and AC excitation on the stator and double-sided reluctance rotors (AFPMG-RR), showing (a) labeled active components and (b) an exploded view of an example design.

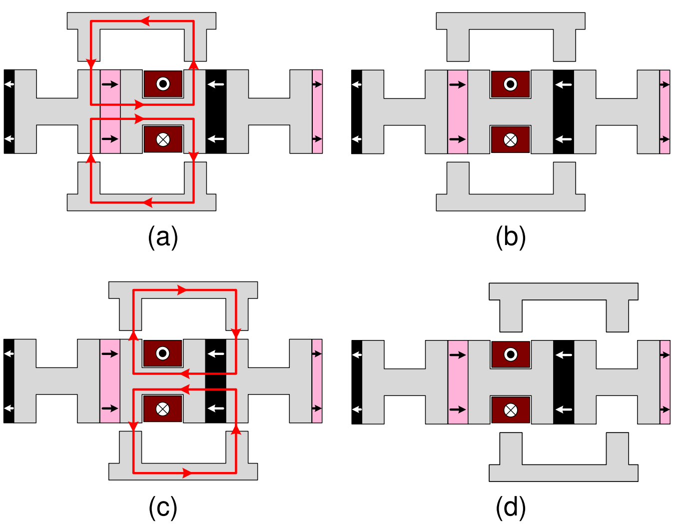

Fig. 3. Operating principle of the proposed AFPMG-RR from a generator-oriented perspective, illustrating positions where flux linkage in the coil is at (a) maximum, (b) zero, (c) minimum, and (d) zero.

be mounted on a lightweight composite material to minimize the overall generator mass.

In coreless stator machines, torque production can be explained by the Lorentz force principle, which describes the interaction between the rotating magnetic field of the rotor and the current-carrying conductors in the stator [28]. Due to the absence of saliency in the stator, the normal force between the rotor and stator is lower than in conventional machines, potentially contributing to a reduction in the overall mass of mechanical components. A normal force still exists between the rotors, and this force becomes increasingly complex as the number of stators and rotors rises to achieve higher power.

B. Single-Sided AFPM Generators

The conventional single-sided AFPM generator (AFPMG) consists of a slotted stator and a surface-mounted PM rotor, as shown in Fig. 2. While it may seem that a double-sided yokeless and segmented armature (YASA) topology could outperform a single-sided structure, Taran *et al.* [25] demonstrated that both configurations deliver similar torque capabilities when using the same PM volume.

The YASA topology is advantageous for high-speed applications, as it replaces the stator yoke with an additional rotor, thereby reducing core losses. However, for low-speed, direct-drive wind turbines, core losses are less critical, and the single-sided design simplifies both manufacturing and mechanical integration of the generator with the wind turbine, making it the preferred structure.

The stator in this design features a tooth tip, which allows adjustments between open- and closed-slot configurations. The stator tooth tip enables a more sinusoidal armature flux density, thereby reducing PM eddy current losses as well as eddy current losses in the stator conductors [29]. Additionally, implementing a stator tooth tip potentially improves cogging torque, torque ripple, and vibration [30].

This study considers two pole-to-slot number ratios for the AFPMG topology. One ratio is 10/12, validated through a low-scale prototype, and the other is the conventional 8/6, which matches the pole-to-slot ratio of the CAFPMGs. For the 10/12 configuration, the pole number is a multiple of 10, while for the 8/6 configuration, it is a multiple of 8.

C. Axial Flux PM Generator with Reluctance Rotor and PM Stator Combined Excitations

This novel AFPM generator features a double-sided reluctance rotor with a modular stator structure that supports both field and armature excitations. The absence of PMs or field excitation windings on the rotor makes the rotor of this AFPMG-RR potentially lighter than conventional CAFPMGs and AFPMGs, which could reduce the overall mass of the rotor's mechanical structure. The stator modules are separated by tangentially magnetized PMs, with AC windings toroidally wound around the back iron of each module.

The tangentially magnetized PMs have alternating magnetization directions in each of two consecutive PMs, resulting in high flux concentration within the stator modules. The toroidal

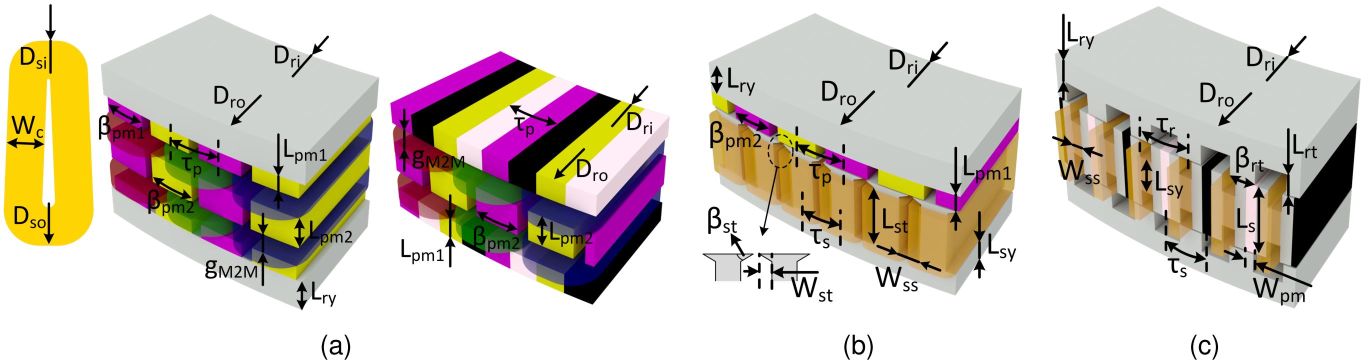

Fig. 5. Geometric design variables applied in the parametric model for the multi-objective optimization, shown for (a) CAFPMGs with surface-mounted PM and Halbach array rotors, (b) conventional AFPMG, and (c) AFPMG-RR configurations.

winding configuration offers a high winding factor and reduces losses due to the shortened end winding. This winding configuration, combined with the modular stator design, facilitates the manufacturing, transportation, and assembly processes, potentially making it a suitable topology for WT generators.

The power generation mechanism of the proposed AFPMG-RR is illustrated in Fig. 3, which shows a straight line diagram corresponding to a part cylindrical surface positioned at the radial center of the stator shown in Fig. 4a. At the rotor position in Fig. 3a, the magnetic circuit reluctance (MCR) reaches its minimum when the rotor teeth align with the stator teeth, maximizing the flux linkage in the coil. As the rotor advances to the position shown in Fig. 3b, MCR is maximized when the rotor teeth align with the PMs, reducing the coil's flux linkage to zero. Upon further rotation to the position depicted in the Fig. 3c, reluctance again decreases, and the flux linkage in the coil reaches its peak, though with reversed polarity due to the change in magnetic flux direction. Finally, in the position illustrated in Fig. 3d, the rotor teeth align with the stator slots, again maximizing reluctance and reducing the coil's flux linkage to zero. This completes one electrical cycle, and the process repeats as the rotor continues rotating, generating a continuous AC output.

One complete electrical cycle corresponds to a single rotor tooth pitch, during which the flux-linkage direction reverses twice. This indicates that the number of rotor teeth in this type of machine is equivalent to the pole pair count of PM rotors in conventional synchronous machines [31]. For the proposed generator in this paper, the rotor tooth-to-slot ratio is 10/12, meaning the rotor has a multiple of ten teeth, corresponding to multiples of 20 magnetic poles.

IV. Problem Formulation and 3D FEA Based Differential Evolution Design Optimization

The direct-drive wind turbine under study targets a rated power of 3 MW at 15 rpm. In such wind turbine generators, key objectives are to minimize mass and maximize efficiency, ensuring cost-effective operation and structural reliability [8], [14], [32]. Therefore, this study employs a dual-objective

TABLE I
Independent optimization variables and their corresponding limits for CAFPMGs with SPM and Halbach array rotors.

Var.	Description	CAFPMG-SPM		CAFPMG-Hal	
		Min.	Max.	Min.	Max.
P	Pole number	80	160	80	160
K_{dr}	Radial length, $\frac{D_{ro}-D_{ri}}{D_{ro}}$	0.10	0.30	0.10	0.30
$K_{L_{PM1}}$	Outer rotor PM length, $\frac{L_{PM1}}{\tau_p}$	0.25	0.55	0.25	0.55
$K_{L_{PM2}}$	Middle rotor PM length, $\frac{L_{PM2}}{\tau_p}$	0.50	1.20	0.50	1.10
$K_{\beta_{PM1}}$	Outer rotor PM arc, $\frac{\beta_{PM1}}{\tau_p}$	0.60	1.00	N/A	N/A
$K_{\beta_{PM2}}$	Middle rotor PM arc, $\frac{\beta_{PM2}}{\tau_p}$	0.60	1.00	0.60	1.00
K_g	Magnet-to-magnet gap, $\frac{g_{M2M}}{\tau_p}$	0.35	0.60	0.35	0.60
K_{oh}	Overhang ratio, $\frac{D_{so}-D_{ro}}{2W_c}$	0.00	1.00	0.00	1.00
K_{ry}	Rotor back iron length, $\frac{L_{ry}}{\tau_p}$	0.25	0.75	N/A	N/A

optimization approach, targeting the minimization of active mass, F_m, and power loss, F_l:

$$F_m = M_{PM} + M_{Cu} + M_{rotor} + M_{stator} \tag{1}$$

$$F_l = P_{Cu} + P_{Fe}. \tag{2}$$

The mass objective function accounts only for the mass of active components, including the PM mass, M_{PM}, copper mass M_{Cu}, rotor core mass M_{rotor}, and stator core mass M_{stator}. The objective function for power loss is determined by summing the generator's losses, where P_{Fe} represents core losses and P_{Cu} represents copper losses. A power factor (P.F.) constraint of 0.7 was applied, ensuring that designs in each generation achieve a P.F. above this threshold.

Each of the AFPM generator topologies considered in this paper has distinct advantages and limitations, as discussed in the topology section. This research aims to evaluate their suitability for direct-drive wind turbines when optimized for the same power rating and performance criteria. While one topology may outperform others in some aspects of this specific application, different design objectives or operational requirements could make another topology more favorable in

TABLE II
INDEPENDENT OPTIMIZATION VARIABLES AND THEIR CORRESPONDING LIMITS FOR CONVENTIONAL AFPMGS WITH 10/12 AND 8/6 POLE-TO-SLOT RATIOS.

Var.	Description	Min.	Max.
P	Pole number	80	160
K_{dr}	Radial length, $\frac{D_{ro}-D_{ri}}{D_{ro}}$	0.10	0.30
$K_{L_{PM1}}$	Rotor PM length, $\frac{L_{PM1}}{\tau_p}$	0.25	0.55
$K_{W_{PM1}}$	Rotor PM arc, $\frac{\beta_{PM1}}{\tau_p}$	0.50	1.00
K_{ry}	Rotor back iron length, $\frac{L_{ry}}{\tau_p}$	0.50	1.00
K_{sy}	Stator yoke length, $\frac{L_{sy}}{\tau_s}$	0.40	1.00
$K_{L_{st}}$	Stator tooth length, $\frac{L_{st}}{\tau_s}$	0.80	2.00
$K_{W_{ss}}$	Stator slot width, $\frac{W_{ss}}{\tau_s}$	0.30	0.80
$K_{W_{st}}$	Stator tooth tip width, $\frac{2W_{st}}{W_{ss}}$	0.10	1.00
$K_{\beta_{st}}$	Stator tooth tip angle, $\frac{\beta_{st}}{90}$	0.10	0.50

alternative scenarios.

Axial flux machines present complex 3D electromagnetic problems, requiring computationally intensive 3D FEA for accurate modeling. Various 2D and quasi-3D modeling approaches have been proposed in the literature to reduce computational costs [28], [33], [34], with examples also available in commercial software such as MotorXP [35]. These methods approximate AFPM machines by slicing them at one or multiple radii and unrolling the sections to create 2D linear models. While such equivalent modeling techniques enable faster calculations, they may introduce inaccuracies, particularly for big AFPM machines with large air-gaps and radial lengths. Large air gaps amplify edge effects, especially in CAFPMGs, which are highly susceptible to air-gap fringing. Additionally, larger radial length increases curvature-related errors, particularly in AFPMG-RR, where the fixed slot dimensions for PMs and windings constrain the tooth width.

In this paper, 3D FEA modeling was chosen for design optimization, with parametric models for AFPM generators developed using Ansys Electronic Desktop software [36]. To manage the large-scale FEA models and expedite the optimization process, matching and symmetry boundary conditions were applied to reduce computational load. The matching boundary conditions allowed the pole number to be an independent variable within the models. Additionally, an ultrafast 3D FEA technique, as described in [37], was employed, requiring a few solutions per cycle to perform the calculations, further enhancing computational speed.

For coreless AFPM generators, applying matching boundary conditions over four pole pitches, $\frac{8\pi}{p}$ (where P is the pole count), along with axial symmetry boundary conditions over half of the machine's axial length, significantly reduced

TABLE III
INDEPENDENT OPTIMIZATION VARIABLES AND THEIR CORRESPONDING LIMITS FOR THE AFPMG-RR.

Var.	Description	Min.	Max.
N_r	Rotor tooth number	80	160
K_{dr}	Radial length, $\frac{D_{ro}-D_{ri}}{D_{ro}}$	0.10	0.30
$K_{L_{rt}}$	Rotor tooth length, $\frac{L_{rt}}{\tau_r}$	0.30	0.80
$K_{W_{rt}}$	Rotor tooth arc, $\frac{\beta_{rt}}{\tau_r}$	0.30	0.70
K_{ry}	Rotor yoke length, $\frac{L_{ry}}{\tau_r}$	0.50	1.00
K_{L_s}	Stator axial length, $\frac{L_s}{\tau_s}$	1.00	3.00
$K_{W_{ss}}$	Stator slot width, $\frac{W_{ss}}{\tau_s}$	0.20	0.70
$K_{L_{sy}}$	Stator slot yoke length, $\frac{L_{sy}}{L_s}$	0.20	0.70
$K_{W_{PM}}$	Stator PM width, $\frac{W_{PM}}{(1-K_{W_{ss}})\tau_s}$	0.30	0.80

computational demand. For a conventional AFPM generator topology with a 10/12 pole-to-slot ratio, the FEA model includes a $\frac{10\pi}{p}$ section, while an 8/6 pole-to-slot ratio includes a $\frac{16\pi}{p}$ section of the full model. Similarly, for an AFPM generator with reluctance rotors and a 10/12 rotor tooth-to-slot ratio, the modeled section contains $\frac{10\pi}{N_r}$, where N_r denotes the rotor tooth count.

These models maintain constant poles, slots, and coils within each modeled portion, enabling the pole number to be treated as an independent variable. The importance of selecting the appropriate pole number has been highlighted in [38] for conventional AFPM machines and in [24] for coreless AFPM machines. These studies demonstrate the significant impact of pole number on mass and efficiency, two critical criteria for direct-drive wind turbine generators. The increment of pole number varies for each generator, such that it is a factor of four for CAFPMGs, a factor of eight or ten for AFPMGs, and a factor of ten for AFPMG-RR.

In radial flux machines, selecting the outer diameter is often straightforward, guided by established examples in the literature and the typical linear scalability of torque production with stack length. However, for AFPM generators used in wind turbines, the literature shows a wide range of outer diameter values, highlighting the need for careful consideration of this parameter in the design optimization process.

The performance of axial flux PM machines highly depends on the outer diameter. The torque equation for AFPM machines indicates that torque has a cubic dependence on outer diameter [10]. In this study, the outer diameter is modeled as a dependent variable of power, ensuring that all candidate designs achieve the specified output power. This approach allows for maintaining a stable current density across designs, which supports effective natural cooling.

The geometrical variables for all proposed AFPM generators are defined and illustrated in Fig. 5, with their respective

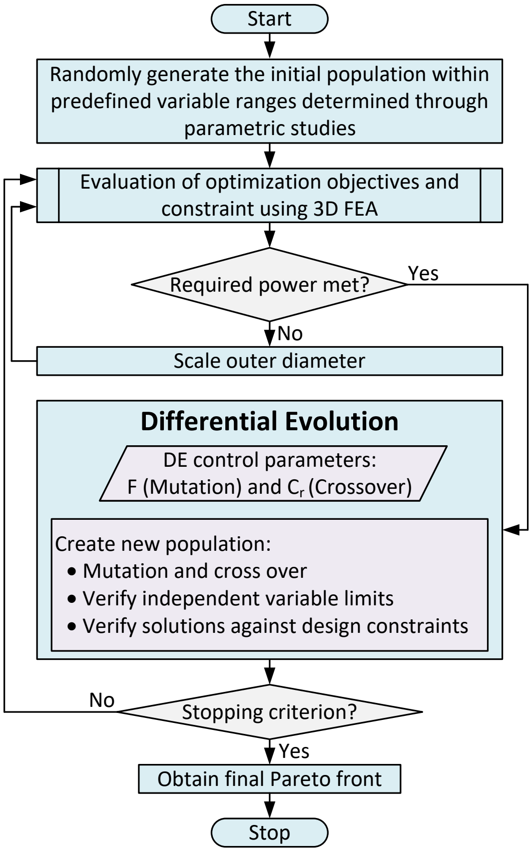

Fig. 6. The proposed optimization algorithm based on the combination of the differential evolution method and 3D FEA.

ranges specified in Tables I to III. The search space for the optimal design is intentionally extensive and is determined through parametric studies aimed at identifying favorable designs. Geometrical constraints are carefully considered to ensure that design variables are limited appropriately, preventing intersections between various geometrical components.

The generators were optimized using the differential evolution (DE) optimization method, which works by iteratively refining a population of candidate solutions, as detailed in [39]. It is a robust, population-based optimization algorithm that offers several advantages over traditional methods. Unlike many optimization techniques, it does not depend on the mathematical characteristics of the problem, making it particularly effective for complex multi-objective optimization challenges, such as the one explored in this study. Its efficient mutation and crossover strategies enable faster convergence, particularly in high-dimensional problems.

Design variable ranges have been carefully determined through multiple parametric studies to ensure the selection of appropriate values, facilitating faster convergence of the optimization process and ensuring the search for the optimal design within a suitable range. The initial values for the j-th design variable of the i-th design in the first generation are randomly generated from this predefined range pool, using:

$$x_{j,i,1} = \text{rand}_j\left(0,1\right) \cdot \left(x_{jU} - x_{jL}\right) + x_{jL}, \tag{3}$$

where X_L and X_U represent the lower and upper bounds of the design space, as specified in Tables I, II, and III. The random selection of design variables for the first generation from a predefined, well-calibrated range significantly reduces the risk of getting trapped in a local optimum. After generating a population of N_P design candidates, the corresponding design objectives and constraints are subsequently evaluated. Then, the vector D containing all design parameters is designated by $X_{i,g}$, where i denotes the population index, and g indicates the generation index.

In order to broaden the search space, each design variable is subjected to a mutation process. The mutation for the j-th design variable is performed using the following approach:

$$v_{j,i,g} = x_{j,r1,g} + F\left(x_{j,r2,g} - x_{j,r3,g}\right), \tag{4}$$

where the indices r_1, r_2, and r_3 are distinct and differ from i. The scale factor F is a positive value greater than zero, with no defined upper limit.

This process generates trial designs, $U_{i,g}$, by combining elements from the designs $X_{i,g}$ and $V_{i,g}$.

$$U_{i,g} = \begin{cases} V_{i,g}, & \text{if rand}\left(0,1\right) \leq CR \\ X_{i,g}, & \text{otherwise,} \end{cases} \tag{5}$$

where CR denotes cross-over probability.

This step is called selection, where the objective function for the trial designs is assessed and compared with that of the target vector to determine an improved target vector for the subsequent generation, as follows:

$$X_{i,g+1} = \begin{cases} U_{i,g}, & \text{if } f\left(U_{i,g}\right) \leq f\left(X_{i,g}\right) \\ X_{i,g}, & \text{otherwise.} \end{cases} \tag{6}$$

The mutation, crossover, and selection processes are iteratively performed until the stopping criteria are met.

The flowchart of the optimization process is illustrated in Fig. 6. A two-step validation was implemented to ensure that each design could consistently achieve the rated power at the specified speed. Initially, the design was evaluated using a preset outer diameter. Based on the discrepancy between the simulated power and the target value, the outer diameter was adjusted accordingly, and the design was re-assessed to confirm that the target power was met. The design variables were initially assigned, and in the second stage, the outer diameter was only scaled within a loop until the design met the rated power requirement.

For electric machine optimization, several approaches ensure that all design candidates produce the same output power. In radial flux machines, torque scales linearly with the machine's stack length. Therefore, the outer diameter is kept constant for applications requiring a fixed outer diameter while the stack length is adjusted linearly, as demonstrated in [8]. Scaling the stack length allows other design variables to

TABLE IV
PERFORMANCE CHARACTERISTICS OF THE OPTIMAL DESIGNS SELECTED FROM THE KNEE REGION OF THE PARETO FRONTS FOR ALL FIVE GENERATOR CONCEPTS, WITH A RATED POWER OF 3 MW AND A SPEED OF 15 RPM.

Generator type	D_{ro} [m]	$\frac{D_{ro}-D_{ri}}{2}$ [m]	Ax. Lgth. [m]	Pole Num. [-]	PM mass [ton]	Spec. TRQ. [Nm/kg]	TRQ. Den. [Nm/L]	Emag. Eff. [%]	P.F. [-]	Goodness [kNm/$\sqrt{W_{loss}}$]
CAFPMG-Hal	7.2	0.25	0.3	160	12.7	99.4	167.8	97.6	0.99	6.930
CAFPMG-SPM	7.4	0.21	0.5	132	8.9	87.0	93.6	97.2	0.98	6.455
AFPMG-10/12	7.3	0.18	0.3	140	3.7	79.0	115.6	97.4	0.78	6.714
AFPMG-8/6	7.8	0.19	0.5	160	2.4	61.1	87.8	96.6	0.74	5.766
AFPMG-RR	6.3	0.49	0.7	90($\times$2)	3.4	35.8	167.3	96.7	0.70	6.124
RFPMG-RR [41]	5.3	N/A	1.9	150	3.6	N/A	11.4	97.2	0.69	5.622
RFPMG-8/12 [41]	5.3	N/A	1.9	150	2.8	N/A	11.4	95.9	0.96	6.620
RFPMG-4/12 [3]	5.1	0.18	1.2	80	1.7	78.8	19.3	96.0	N/A	5.374
RFPMG-RR [8]	5.0	N/A	2.0	120	N/A	38.2	12.2	97.2	0.9	6.473

remain constant as determined by the optimization process. Additionally, the current density is maintained at a constant level for all design candidates, ensuring compatibility with the motor's cooling system.

Another approach involves scaling the current density to achieve the required torque, as presented in [40]. This method may be helpful when the stack length is constrained in radial flux machines or when applied to coreless stator machines. In radial flux machines, however, scaling of current density can lead to core saturation, beyond which further increases do not enhance torque. In contrast, torque scales linearly with current density for coreless stator machines, making this approach more straightforward. The primary limitation is ensuring design candidates adhere to the maximum allowable current density.

In this study, neither of these methods is selected, as the radial length in AFPM machines—analogous to stack length in radial flux machines—does not exhibit a linear relationship with torque due to curvature effects. Moreover, scaling the current density introduces cooling challenges and saturation concerns for the considered generators. Instead, this paper proposes a novel strategy according to the torque equation for AFPM machines, which is scaling the outer diameter. Adjusting the outer diameter to achieve the required power addresses cooling and saturation concerns while ensuring a fair comparison across all proposed topologies.

V. OPTIMIZATION RESULTS, DISCUSSION, AND EXPERIMENTAL VALIDATIONS

The five proposed AFPM generator designs were optimized using the described process, with fifty design candidates per generation to allow for a comprehensive exploration of the design space. The optimization results for the conflicting objectives are shown in Fig. 7, where each scatter point is color-coded based on the PM mass, a factor that significantly influences the generator's cost.

A comparison of the Pareto fronts for the CAFPMGs shows that the configuration with outer Halbach array PM rotors

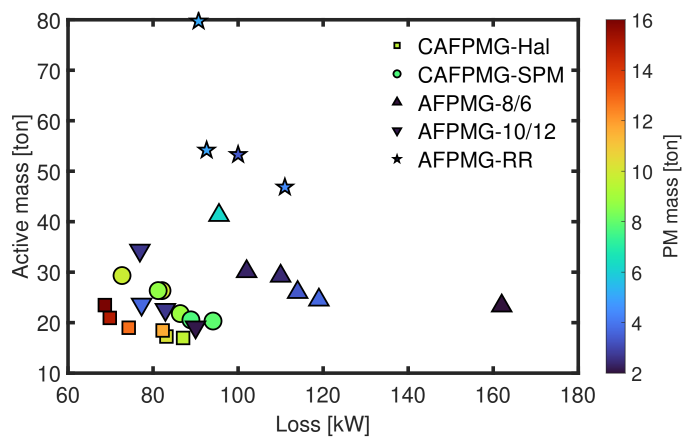

Fig. 7. Pareto front design candidates for all five generator concepts, with all designs rating 3 MW of power at 15 rpm.

outperforms the SPM outer rotor design in both optimization objectives. This improved Halbach array rotor variant performance comes with a 40-60% increase in PM mass. While the CAFPMG-Hal demonstrates superior efficiency and reduced mass relative to other optimized AFPM generators, it is essential to note that both CAFPMG configurations require a higher PM mass to reach these performance levels.

The comparison of the Pareto fronts for conventional AFPMGs shows that designs with a 10/12 pole-to-slot ratio outperform those with an 8/6 ratio in terms of power losses. This suggests that while the 8/6 configuration performs better than the 10/12 in coreless AFPM designs [27], the situation is reversed for AFPM machines with a stator core. The differences in power losses for 8/6 and 10/12 are potentially due to the lower winding factor of the 8/6 configuration, as noted in [42].

The Pareto front results for the AFPMG-RR highlight the significantly higher mass of this generator configuration compared to other AFPM generators. This is likely due to the limited slot space available for windings in the stator, as

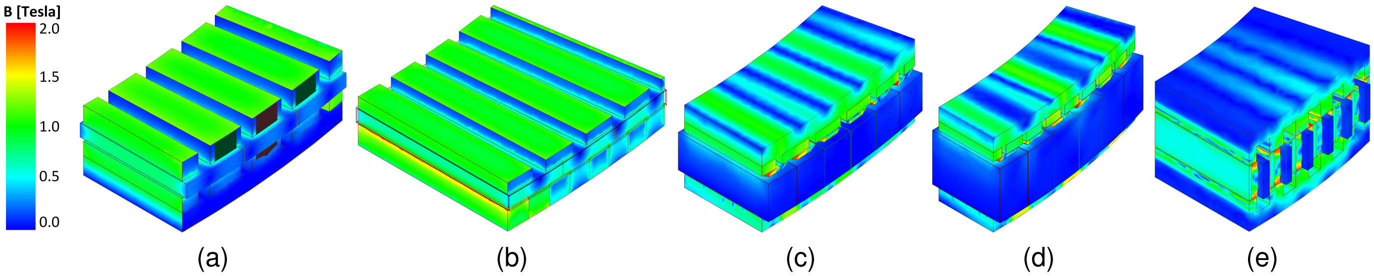

Fig. 8. Flux density distributions for the optimal designs of (a) the half-axial model of CAFPMG-SPM, (b) the half-axial model of CAFPMG-Hal, (c) AFPMFG-10/12, (d) AFPMFG-8/6, and (e) AFPMG-RR.

the PMs are integrated within the stator for this configuration. This constraint on the available space restricts the electrical loading and may negatively affect the machine's torque [43].

The optimal designs for each generator were selected at the knee region of their respective Pareto fronts. The corresponding designs' flux density distributions are illustrated in Fig. 8, with their specifications detailed in Table IV. A comparison of the outer diameters reveals that although the optimal design for the AFPMG-RR has an outer diameter of 6.3 m, which is smaller than those of the other topologies, with an average outer diameter of 7.5 m, the axial and radial lengths of this generator is larger. These increases can be due to the AFPMG-RR's tendency to have a larger axial length to accommodate two rotors with required saliency and to compensate for its lower electrical loading.

The radial lengths of the optimal designs are relatively small in comparison to the outer diameters. While increasing the radial length in AFPM machines enhances torque production [28], it results in designs that are less efficient in terms of active material usage.

A comparison of specific torque density and torque density demonstrates the superior performance of the CAFPMG-Hal, which can be attributed to the larger PM mass and the absence of ferromagnetic cores. Notably, although the CAFPMG-SPM achieves a higher specific torque density than the AFPMG-10/12, it has a lower overall torque density. This difference is essential for mechanical design, as higher torque density may enable the use of smaller and lighter mechanical components.

The power factor for coreless AFPM generators is close to unity, while for other AFPMGs, it ranges around 0.7. The goodness comparison shows that, except for the CAFPMG-Hal, the AFPMG-10/12 offers higher goodness and even outperforms the CAFPMG-SPM. This can be explained by the fact that in low-speed operations—such as those considered in this study—core losses are negligible compared to copper losses, allowing the conventional AFPMG to outperform the coreless variant.

The second half of Table IV presents data on radial flux PM generators (RFPMGs) for direct-drive wind turbines with the same power rating from existing literature. From a dimensional perspective, AFPM machines exhibit an average outer diameter approximately 40% larger than RFPMGs, while their axial length is nearly four times shorter than the RFPMG examples listed. Given that the listed RFPMGs share a similar topology with the AFPMG-10/12, AFPMG-8/6, and AFPMG-RR, the PM mass for both AFPMGs and RFPMGs with the same rating appears to be comparable.

A comparison of specific torque suggests that both topologies can achieve similar values, with AFPMGs slightly performing better. The torque density analysis highlights a significant advantage of AFPMGs over RFPMGs. This advantage is crucial, as a smaller volume simplifies mechanical integration, installation, and transportation. Additionally, it reduces the mass of the generator's mechanical support structure, further lowering costs and manufacturing complexity. The smaller axial length of AFPMGs allows for adding multiple units on the same shaft, enabling higher power output within the same volume as a single RFPMG, which would otherwise produce only a fraction of that power.

A. Experimental Validation and Analysis of Mass and Cost

A common approach for experimentally verifying wind turbine generators is to construct a significantly downscaled prototype and scale its performance based on the torque relationship with the outer diameter and stack length in radial flux machines or with the outer diameter and radial length in AFPM machines. For example, Lehr *et al.* [41] designed a 3 MW direct-drive wind turbine generator by scaling the dimensions of a 45 kW prototype. In this paper, the 3D FEA models used for the design optimization of the proposed generators have been calibrated using low-scaled prototypes previously developed by the same research group [25], [26]. To further validate the calculations, other AFPM machine prototypes, including both high- and low-power prototypes and industrial products, have been numerically compared to the optimized AFPMGs presented in this work. Parameters such as specific torque, torque constant, and efficiency further support the experimental verification and enhance confidence in the results.

The FEA models developed for the CAFPMG-SPM, and AFPMG-10/12 were validated using low-scale reference prototypes from this research group, as illustrated in Figs. 9a and 9b and documented across multiple studies. In [26], the CAFPMG-SPM reference design was employed to validate stator eddy current losses at high speeds, copper losses, and torque. Similarly, the AFPMG-10/12 reference design,

TABLE V
EXPERIMENTALLY MEASURED AND CALCULATED PARAMETERS FOR THE LOW-SCALED PROTOTYPES OF THE CORELESS STATOR AFPM MACHINE WITH SPM ROTOR AND THE CONVENTIONAL AFPMG-10/12.

Generator type [-]	Analysis [-]	P_{out} [kW]	OD [mm]	Ax. Lgth. [mm]	TRQ. [Nm]	TRQ. Con. [Nm/A]	R [mΩ]	Eff. [%]	Spec. TRQ. [Nm/kg]
CAFPMG-SPM [14]	-	6×10^3	20×10^6	-	5×10^6	-	-	-	80
CAFPMG-SPM [19]	FEA Exp	1000	6×10^3	356	796	-	-	93.6	-
CAFPMG-SPM [26]	FEA	4.2	310	35	19.0	2.2	550	95.8	2.3
	Exp				18.1	2.2	570	95.8	-
CAFPMG-Hal [44]	FEA	5.8	310	35	24.0	3.1	550	97.5	3.2
CAFPMG-Hal [45]	Exp	6	190	-	9.2	-	-	-	9.8
AFPMG-10/12 [25]	FEA	7.7	200	-	21.1	0.9	56	94.0	5.6
	Exp				20	0.9	59	91.0	-

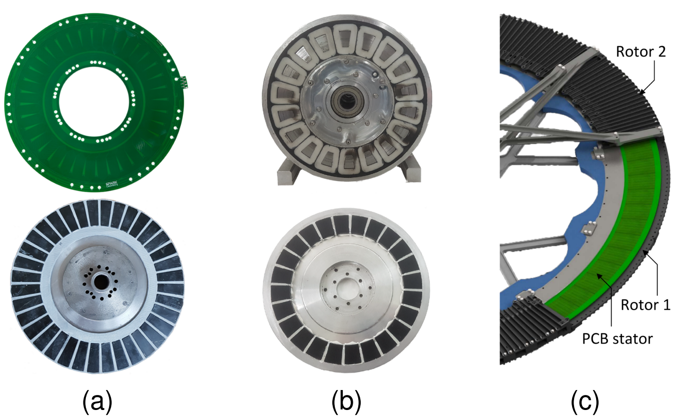

Fig. 9. Coreless stator AFPM machine prototype with surface-mounted PM rotor (a), the conventional single-sided AFPM machine prototype (b), and the coreless AFPM genrator with PCB stator designed by Boulder Wind Power, used for the verification of the developed FEA models and calculations.

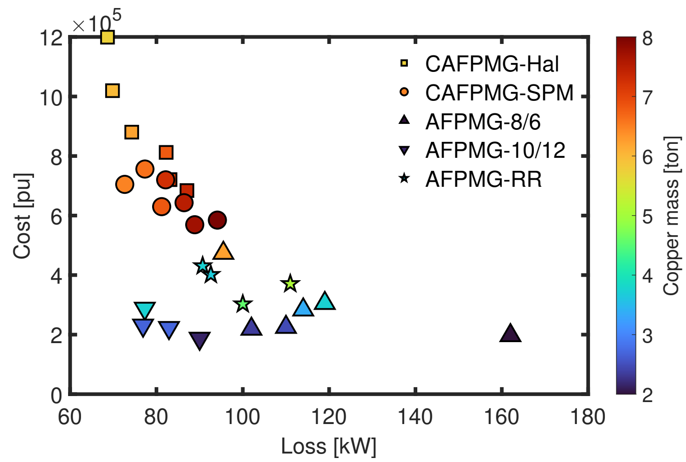

Fig. 10. Pareto front design candidates for all five generator concepts, plotted based on a consistent per-unit cost system.

introduced and optimized in [25], verified the accuracy of torque, copper losses, and core losses. The close agreement between experimental measurements and FEA results supports the reliability of the FEA models presented in this study.

The coreless AFPM generator with a PCB stator, developed by Boulder Wind Power [14] and depicted in Fig. 9c, is used to further validate the calculations for CAFPMG-SPM at high power levels similar to those presented in this study. The specific torque of the Boulder CAFPMG is within the same range as the optimal design achieved in this work.

The validated FEA model for the CAFPMG-SPM was subsequently adapted to a Halbach array rotor variant in [44], maintaining comparable size and ratings. This adaptation confirmed the Halbach array rotor's advantage in mass reduction. Additionally, a coreless AFPM machine from LaunchPoint Electric Propulsion Solutions, Inc. [45] was used to assess and compare the specific torque capabilities of CAFPMGs with SPM and Halbach array rotors. The data comparing the experimental and 3D FEA simulations of the described reference prototypes are listed in Table V.

The Pareto fronts in Fig. 7 show that the CAFPMG-Hal achieves the lowest mass among all the AFPMGs considered, aligning well with the experimental validations in Table V. Furthermore, the Pareto front comparison reveals that CAFPMG-SPM and AFPMG-10/12 exhibit similar mass performance, although the CAFPMG-SPM requires a higher PM mass. Therefore, comparing the costs of active components on a consistent scale becomes increasingly important.

Based on the cost model examples provided in [39], the cost of active materials for AFPM generators can be approximated per unit mass of steel as follows:

$$F_c = 65 \cdot m_{PM} + 8 \cdot m_{Cu} + m_c, \tag{7}$$

where m_{PM}, m_{Cu}, and m_c denote the masses of PM, copper, and steel.

The Pareto front designs for each generator regarding cost and loss are presented in Fig. 10. These results highlight that CAFPMG-Hal is significantly more costly due to the high

TABLE VI
LOSS BREAKDOWN FOR THE SELECTED OPTIMAL DESIGNS OF ALL GENERATORS, HIGHLIGHTING THE LOW CONTRIBUTION OF CORE LOSS TO THE TOTAL LOSS IN CORED AFPM GENERATORS DUE TO THE LOW SPEED.

	Copper loss [kW]	Core loss [kW]
CAFPMG-Hal	77.3	N/A
CAFPMG-SPM	86.4	0.0
AFPMG-10/12	75.4	7.5
AFPMG-8/6	96.2	6.2
AFPMG-RR	87.7	12.4

mass of PMs in this configuration. Meanwhile, a cost comparison between CAFPMG-SPM and AFPMG-10/12—two designs with similar mass and loss characteristics, as shown in Fig. 7—reveals that AFPMG-10/12 achieves comparable losses to CAFPMG-SPM at just one-third of the cost.

Each design in Fig. 10 is color-coded to represent copper mass. A comparison between CAFPMG-SPM and AFPMG-10/12 reveals that CAFPMG-SPM's higher cost is not solely due to its greater PM mass; the increased copper mass also plays a significant role. Given that copper is approximately six times more costly than steel, this added copper mass substantially contributes to CAFPMG-SPM's higher cost.

B. Loss

A breakdown of the loss components for the selected optimal designs is presented in Table VI, detailing the proportions of copper and core losses. In CAFPMG-SPM, core loss is nearly negligible due to the minimal armature reaction typical of coreless stator machines. The core losses in the cored AFPMGs account for approximately 10% of the total losses. The low-speed operation of direct-drive wind turbine generators contributes to reduced core loss, a characteristic that does not hold for high-speed applications such as propulsion systems. This advantage allows conventional cored generators, such as the AFPMG-10/12, to achieve efficiencies comparable to those of coreless designs.

Although core losses are negligible in the rotor back iron of coreless machines, eddy current and circulating current losses in the conductors can be substantial. For direct-drive wind turbine generators with low fundamental frequencies, eddy current losses in the proposed CAFPMGs are likely minor, provided that conductor size is optimally selected. However, circulating current losses presents a different challenge.

The airgap size in the CAFPMGs is likely large enough to accommodate as much conductor as needed to produce the required power, leading to conductor layers being stacked axially. This arrangement results in varying distances from the rotor surface for each conductor layer, exposing them to different magnetic flux densities. The resulting induced voltages vary across layers, creating circulating currents between them.

These circulating currents generate losses in the conductors, which can be considerable given the large airgap and conductor volume. To reduce these losses, conductor transposition is

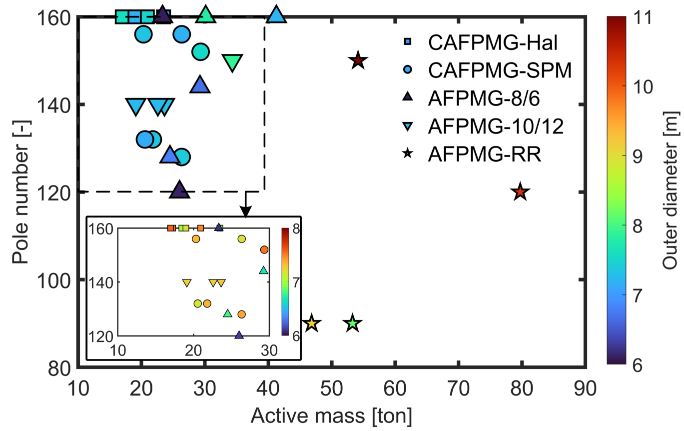

Fig. 11. Pareto front design candidates plotted in terms of pole number and outer diameter, showing a trend where designs with lower mass tend to have larger outer diameters and higher pole numbers.

recommended to balance the overall back-EMF across layers. Alternatively, Litz wire, with its twisted structure, can also mitigate these losses, though its higher cost further increases the overall cost of CAFPMGs.

In the proposed AFPMGs, PM eddy current losses are minimal, not only due to the generator's low fundamental frequency but also because of PM segmentation. Given the large magnet sizes, segmentation is applied in radial, axial, and tangential directions, with radial and axial segmentation particularly effective in reducing eddy current losses. For CAFPMGs, these losses are even further minimized due to the low armature reaction.

C. Effects of Outer Diameter and Pole Number

The Pareto front designs of the proposed AFPM generators, considering pole number and mass, are shown in Fig. 11. These results indicate that designs with higher pole numbers tend to have lower mass. Previous studies [38], [40] have demonstrated that increasing the pole number enhances specific torque density, but it also reduces both magnetic and current loading within a fixed machine envelope. This reduction in loading can potentially lead to decreased efficiency if the current density is scaled up to meet the required power.

In the optimization process presented in this paper, the current density was kept constant across all designs to ensure the effective cooling of the proposed generators. The outer diameter was adjusted to meet the power requirements. In Fig. 11, each design is color-coded to represent the outer diameter. The results suggest that the optimal designs favor higher pole numbers and larger outer diameters until a balance is reached between increasing the outer diameter and reducing the pole number to minimize mass.

VI. CONCLUSION

This paper has proposed, optimized, and systematically compared four distinct axial flux permanent magnet generator (AFPM) concepts in terms of mass, cost, and efficiency. The optimization and comparison were carried out using 3D

FEA models and differential evolution optimization algorithm. Experimental prototypes for the coreless and conventional designs were used to validate their respective FEA models, which were subsequently adapted for the other variants. For each topology, an example generator was designed and optimized with identical power and speed ratings. This allowed for a fair comparison in terms of active material cost and mass, with simulated results provided for efficiency.

The resulting performance indicated that the coreless design with a Halbach array PM rotor achieved superior mass, efficiency, and torque density. However, it required a significantly higher volume of PM material, making it the least cost-effective option. In contrast, the conventional 10/12 pole-to-slot ratio design demonstrated a strong balance, achieving competitive performance in terms of mass and efficiency while outperforming the coreless design with surface-mounted PM rotors, in terms of cost, PM volume, and overall cost-effectiveness. The 8/6 pole-to-slot ratio conventional design, though similar in mass to the 10/12 variant, experienced higher losses due to a lower winding factor. The efficiency in conventional designs benefited from minimized core loss due to the low operational speed typical in direct-drive wind turbines. The axial flux variant with reluctance rotors exhibited limitations in mass and efficiency, likely resulting from restricted slot space for windings, which limited electrical loading and reduced achievable torque relative to other designs.

Acknowledgment

This paper is based upon work supported by the National Science Foundation (NSF) under Award No. #1809876. The support for Donovin Lewis through an NSF Fellowship under Grant No. 2239063, and of ANSYS Inc., and University of Kentucky, the L. Stanley Pigman Chair in Power Endowment is also gratefully acknowledged. Any findings and conclusions expressed herein are those of the authors and do not necessarily reflect the views of the NSF.

References

[1] International Renewable Energy Agency (IRENA), "Renewable capacity statistics 2023," 2023. [Online]. Available: https://www.irena.org/Publications/2023/06/Renewable-Capacity-Statistics-2023

[2] M. Alberg and S. Tinker, "Recent advancements in wind power generation technology," *Journal of Renewable Energy*, vol. 35, no. 3, pp. 45–58, 2019.

[3] H. Polinder, F. F. Van der Pijl, G.-J. De Vilder, and P. J. Tavner, "Comparison of direct-drive and geared generator concepts for wind turbines," *IEEE Transactions on Energy Conversion*, vol. 21, no. 3, pp. 725–733, 2006.

[4] A. K. Papatzimos, T. Dawood, and P. R. Thies, "Data insights from an offshore wind turbine gearbox replacement," in *Journal of physics: Conference series*, vol. 1104, no. 1. IOP Publishing, 2018, p. 012003.

[5] T. Husain, I. Hasan, Y. Sozer, I. Husain, and E. Muljadi, "Design considerations of a transverse flux machine for direct-drive wind turbine applications," *IEEE Transactions on Industry Applications*, vol. 54, no. 4, pp. 3604–3615, 2018.

[6] J. H. Potgieter and M. J. Kamper, "Double PM-rotor, toothed, toroidal-winding wind generator: A comparison with conventional winding direct-drive PM wind generators over a wide power range," *IEEE Transactions on Industry Applications*, vol. 52, no. 4, pp. 2881–2891, 2016.

[7] P. M. Tlali, R.-J. Wang, S. Gerber, C. D. Botha, and M. J. Kamper, "Design and performance comparison of Vernier and conventional PM synchronous wind generators," *IEEE Transactions on Industry Applications*, vol. 56, no. 3, pp. 2570–2579, 2020.

[8] A. Mohammadi, O. A. Badewa, Y. Chulaee, D. D. Lewis, S. Essakiappan, M. Manjrekar, and D. M. Ionel, "Design optimization of a direct-drive wind generator with a reluctance rotor and a flux intensifying stator using different PM types," *IEEE Transactions on Industry Applications*, 2024.

[9] F. Blaabjerg and D. M. Ionel, "Renewable energy devices and systems–state-of-the-art technology, research and development, challenges and future trends," *Electric Power Components and Systems*, vol. 43, no. 12, pp. 1319–1328, 2015.

[10] J. F. Gieras, R.-J. Wang, and M. J. Kamper, *Axial Flux Permanent Magnet Brushless Machines*. Dordrecht: Springer Netherlands Springer e-books, 2008.

[11] F. Nishanth, J. Van Verdeghem, and E. L. Severson, "A review of axial flux permanent magnet machine technology," *IEEE Transactions on Industry Applications*, vol. 59, no. 4, pp. 3920–3933, 2023.

[12] E. Muljadi, C. P. Butterfield, and Y.-H. Wan, "Axial-flux modular permanent-magnet generator with a toroidal winding for wind-turbine applications," *IEEE Transactions on Industry Applications*, vol. 35, no. 4, pp. 831–836, 1999.

[13] M. B. Jore, L. Jore, M. A. Kvam, J. D. Jore, D. Samsel, J. D. Duford, and J. S. Smith, "Systems and methods for improved direct drive generators," Oct. 6 2015, uS Patent 9,154,024.

[14] S. Butterfield, J. Smith, D. Petch, B. Sullivan, P. Smith, and K. Pierce, "Advanced gearless drivetrain-phase I technical report," Boulder Wind Power, Inc., Tech. Rep., 2012.

[15] R. Neumann, R. Anbarasu, N. C. Olsen, J. F. Eastham, and R. J. Hill-Cottingham, "Direct drive segmented generator," Patent WO2 012 059 109A2, 2012. [Online]. Available: https://patentscope.wipo.int/search/en/detail.jsf?docId=WO2012059109&_cid=P22-M4HFNV-63037-1

[16] M. Vatani, A. Mohammadi, D. Lewis, J. F. Eastham, and D. M. Ionel, "Coreless axial flux Halbach array permanent magnet generator concept for direct-drive wind turbine," in *2023 12th International Conference on Renewable Energy Research and Applications (ICRERA)*. IEEE, 2023, pp. 612–617.

[17] B. Chalmers and E. Spooner, "An axial-flux permanent-magnet generator for a gearless wind energy system," *IEEE Transactions on Energy Conversion*, vol. 14, no. 2, pp. 251–257, 1999.

[18] P. Jaen-Sola, A. S. McDonald, and E. Oterkus, "Dynamic structural design of offshore direct-drive wind turbine electrical generators," *Ocean Engineering*, vol. 161, pp. 1–19, 2018.

[19] O. Ubani, "Improving the torque density of C-GEN direct drive axial flux air cored permanent magnet generator," Ph.D. dissertation, University of Edinburgh, 2021.

[20] M. Vatani, Y. Chulaee, J. F. Eastham, X. Pei, and D. M. Ionel, "Multi-wound axial flux generators with Halbach array rotors," in *2024 IEEE Energy Conversion Congress and Exposition (ECCE)*, 2024, pp. 1–6.

[21] A. McDonald, N. Al-Khayat, D. Belshaw, M. Ravilious, A. Kumaraperumal, A. Benatamane, M. Galbraith, D. Staton, K. Benoit, and M. Mueller, "1mw multi-stage air-cored permanent magnet generator for wind turbines," 2012.

[22] M. A. Mueller, J. Burchell, Y. C. Chong, O. Keysan, A. McDonald, M. Galbraith, and E. J. E. Subiabre, "Improving the thermal performance of rotary and linear air-cored permanent magnet machines for direct drive wind and wave energy applications," *IEEE Transactions on Energy Conversion*, vol. 34, no. 2, pp. 773–781, 2018.

[23] L. M. Jore and M. B. Jore, "Conductor optimized axial field rotary energy device," Sep. 19 2006, uS Patent 7,109,625.

[24] M. Vatani, J. F. Eastham, and D. M. Ionel, "Multi-disk coreless axial flux permanent magnet synchronous motors with surface PM and Halbach array rotors for electric aircraft propulsion," in *IEEE Energy Conversion Congress & Expo (ECCE)*. IEEE, 2024.

[25] N. Taran, D. Klink, G. Heins, V. Rallabandi, D. Patterson, and D. M. Ionel, "A comparative study of yokeless and segmented armature versus single sided axial flux PM machine topologies for electric traction," *IEEE Transactions on Industry Applications*, vol. 58, no. 1, pp. 325–335, 2021.

[26] Y. Chulaee, G. Heins, B. Robinson, A. Mohammadi, M. Thiele, D. Patterson, and D. M. Ionel, "Design and optimization of high-efficiency coreless PCB stator axial flux PM machines with minimal eddy and

circulating current losses," *IEEE Transactions on Industry Applications*, pp. 1–13, 2024.

[27] S. P. Colyer, P. Arumugam, and J. F. Eastham, "Modular airgap windings for linear permanent magnet machines," *IET Electric Power Applications*, vol. 12, no. 7, pp. 953–961, 2018.

[28] M. Vatani, Y. Chulaee, J. F. Eastham, and D. M. Ionel, "Analytical and fe modeling for the design of coreless axial flux machines with Halbach array and surface PM rotors," in *2024 IEEE Energy Conversion Congress and Exposition (ECCE)*, 2024, pp. 1–7.

[29] I. Afinowi, Z. Zhu, Y. Guan, J. Mipo, and P. Farah, "Electromagnetic performance of stator slot permanent magnet machines with/without stator tooth-tips and having single/double layer windings," *IEEE Transactions on Magnetics*, vol. 52, no. 6, pp. 1–10, 2016.

[30] Y.-J. Won, J.-H. Kim, S.-M. An, and M.-S. Lim, "Comparative study of cogging torque, torque ripple and vibration on stator tooth chamfer types in permanent magnet synchronous motors," *IEEE Transactions on Magnetics*, 2024.

[31] Z. Zhu and J. Chen, "Advanced flux-switching permanent magnet brushless machines," *IEEE transactions on magnetics*, vol. 46, no. 6, pp. 1447–1453, 2010.

[32] W. Gul, Q. Gao, and W. Lenwari, "Optimal design of a 5-mw double-stator single-rotor pmsg for offshore direct drive wind turbines," *IEEE Transactions on Industry Applications*, vol. 56, no. 1, pp. 216–225, 2019.

[33] M. Gulec and M. Aydin, "Implementation of different 2d finite element modelling approaches in axial flux permanent magnet disc machines," *IET Electric Power Applications*, vol. 12, no. 2, pp. 195–202, 2018.

[34] J. R. Bumby, R. Martin, M. Mueller, E. Spooner, N. Brown, and B. Chalmers, "Electromagnetic design of axial-flux permanent magnet machines," *IEE Proceedings-Electric Power Applications*, vol. 151, no. 2, pp. 151–160, 2004.

[35] MotorXP, "Electric motor design software." [Online]. Available: https://motorxp.com/#motorpm

[36] *Ansys® Electronics, Maxwell, version 24.1, 2024, ANSYS Inc.*

[37] D. M. Ionel and M. Popescu, "Ultrafast finite-element analysis of brushless pm machines based on space–time transformations," *IEEE Transactions on Industry Applications*, vol. 47, no. 2, pp. 744–753, 2010.

[38] N. Taran, V. Rallabandi, G. Heins, and D. M. Ionel, "Systematically exploring the effects of pole count on the performance and cost limits of ultrahigh efficiency fractional HP axial flux PM machines," *IEEE Transactions on Industry Applications*, vol. 56, no. 1, pp. 117–127, 2019.

[39] M. Rosu, P. Zhou, D. Lin, D. M. Ionel, M. Popescu, F. Blaabjerg, V. Rallabandi, and D. Staton, *Multiphysics simulation by design for electrical machines, power electronics and drives*. John Wiley & Sons, 2017.

[40] M. Vatani, Y. Chulaee, A. Mohammadi, D. R. Stewart, J. F. Eastham, and D. M. Ionel, "On the optimal design of coreless AFPM machines with Halbach array rotors for electric aircraft propulsion," in *2024 IEEE Transportation Electrification Conference and Expo (ITEC)*. IEEE, 2024, pp. 1–6.

[41] M. Lehr, D. Dietz, and A. Binder, "Electromagnetic design of a permanent magnet flux-switching-machine as a direct-driven 3 mw wind power generator," in *2018 IEEE International Conference on Industrial Technology (ICIT)*. IEEE, 2018, pp. 383–388.

[42] J. F. Eastham, T. Cox, and J. Proverbs, "Application of planar modular windings to linear induction motors by harmonic cancellation," *IET electric power applications*, vol. 4, no. 3, pp. 140–148, 2010.

[43] H. Chen, A. M. EL-Refaie, and N. A. Demerdash, "Flux-switching permanent magnet machines: A review of opportunities and challenges—part i: Fundamentals and topologies," *IEEE Transactions on Energy Conversion*, vol. 35, no. 2, pp. 684–698, 2019.

[44] Y. Chulaee, D. Lewis, M. Vatani, J. F. Eastham, and D. M. Ionel, "Torque and power capabilities of coreless axial flux machines with surface PMs and Halbach array rotors," in *2023 IEEE International Electric Machines & Drives Conference (IEMDC), San Francisco, CA*. IEEE, 2023, pp. 1–6.

[45] LaunchPoint Electric Propulsion Solutions, Inc. [Online]. Available: https://launchpointeps.com/motors-generators/

Matin Vatani (Graduate Student Member, IEEE) received his M.Sc. degree in Electrical Engineering, with a focus on Power Electronics and Electrical Machines, from Amirkabir University of Technology (Tehran Polytechnic), Tehran, Iran, in 2020. He is currently pursuing a Ph.D. in Electrical and Computer Engineering at the University of Kentucky, where he is a graduate research assistant in the SPARK Laboratory. His work is supported by NASA, NSF, and industry-funded projects. His research has been recognized with multiple academic honors and awards for papers and experimental demonstrations. His research interests include advanced electromagnetic finite element analysis (FEA), electric machine design optimization, and power electronic drives.

Ali Mohammadi (Member, IEEE) received his B.Sc. and M.Sc. degrees in electrical engineering from Babol Noshirvani University of Technology, Iran, in 2016 and 2020, respectively, and his Ph.D. from the University of Kentucky, USA, in 2025. His research focuses on electric machine design, motor drives, power electronics, transportation electrification, and renewable energy systems.

He has contributed to NSF-, NASA-, and industry-sponsored projects and received multiple honors, including the IEEE Transactions on Energy Conversion Best Paper Award. He was recognized with Best Paper Awards at the 2022 IEEE International Conference on Renewable Energy Research and Applications (ICRERA), the 2023 IEEE Transportation Electrification Conference (ITEC), and the 2023 IEEE ICRERA. He also received Best Student Demonstration Awards at the 2024 IEEE Energy Conversion Congress and Exposition (ECCE) and the 2025 IEEE International Electric Machines and Drives Conference (IEMDC).

Donovin D. Lewis (Graduate Student Member, IEEE) received the B.Sc. degree in electrical engineering in 2021 from the University of Kentucky (UKY), Lexington, KY, USA, where he is working towards the Ph.D. degree with the SPARK Laboratory, Department of Electrical and Computer Engineering as a National Science Foundation (NSF) Graduate Research Fellow and Lighthouse Beacon Foundation Graduate Research Fellow. He also received the Otis A. Singletary Graduate Fellowship at UKY, and paper and student demonstration awards at IEEE international conferences. Mr. Lewis is also a remote research collaborator with the Oak Ridge National Laboratory, and a summer visitor with the University of Oxford, Oxford, England. His research interests include design and development of wireless charging systems and electric motors.

John Frederic Eastham received the BSc, MSc, Ph.D., and D.Sc. degrees from University of Manchester, U.K. He was a Reader with Imperial College in London, Professor with Aberdeen University, and then Professor and Head of Department at University of Bath, U.K., where he subsequently served as Dean and Pro Vice Chancellor, and is currently Emeritus Professor.

Professor Eastham does much of his work with industry. He was a main board Director of the Mycalex Group Company and a member of the UK Technology Strategy Board. He has worked as a consultant for many companies including Goodrich Aerospace, Force Engineering Ltd, Vestas Wind Systems Ltd and General Electric Global Research. He is the author or co-author of more than 45 patents and 200 technical papers. His public committee work has included chairmanship of the UK Science and Engineering Research Council Electrical Engineering Committee, and membership of the Council for National Academic Awards in the U.K.

Professor Eastham is a Fellow of the Royal Society of Edinburgh, of the Royal Academy of Engineering, and of the Institution of Engineering and Technology (IET) in the U.K. He received a Doctorate Honoris Causa from Bucharest University, Romania, and was appointed Honorary Professor by Harbin University and CUMT University in China. He was awarded the Institution of Electrical Engineers Achievement Medal in the Science, Education and Technology Division, and is a recipient of the Powergen Partnership Award, and of the Lifetime Contribution to Magnetics Award from the UK Magnetics Society.

Dan M. Ionel (Fellow, IEEE) received both the M.Eng. and Ph.D. degrees in electrical engineering from the Polytechnic University of Bucharest, Bucharest, Romania. His doctoral studies included a Leverhulme Visiting Fellowship with the University of Bath, Bath, U.K. He was a Postdoctoral Researcher with the SPEED Laboratory, University of Glasgow, Glasgow, U.K.

Previously to 2015, he worked in industry, most recently as Chief Engineer with Regal Beloit Corp., Grafton, WI, USA, and before that as Chief Scientist with Vestas Wind Turbines. He was also a Visiting Professor and a Research Professor with the University of Wisconsin and Marquette University, Milwaukee, WI, USA. He is currently Professor and the L. Stanley Pigman Chair in Power with the University of Kentucky, Lexington, KY, USA, where he is also the Director of the Power and Energy Institute of Kentucky and of the SPARK Laboratory. During his 2024 sabbatical in England, U.K., he was a Leverhulme Visiting Professor with University of Bath, expanding also the collaboration with University of Oxford, and was appointed as an Honorary Professor at University College London (UCL).

Dr. Ionel has contributed to technological developments with long-lasting industrial impact, designed electric machines and drives with ratings between 0.002 and 10,000hp. He holds more than 40 patents, and has authored or coauthored two books and more than 300 technical papers, including IEEE award winners. He served as chair of large committees and conferences for the IEEE power societies, and editor of journals. Dr. Ionel received the Cyril G. Veinott Award, the highest distinction for electromechanical energy conversion contributions from the IEEE PES.